Broadband shifting luminescence in Cr^{3+}/Yb^{3+} codoped $Y_3Al_5O_{12}$ thin films by pulsed laser deposition

Yinzhen Wang (王银珍)[1,*], Ning Li (李 宁)[1], Pingping Duan (段萍萍)[1], Junyong Deng (邓俊勇)[2], Liaolin Zhang (张料林)[2], Benli Chu (初本莉)[1], and Qinyu He (何琴玉)[1]

[1]*Guangdong Provincial Key Laboratory of Quantum Engineering and Quantum Materials, School of Physics and Telecommunication Engineering, South China Normal University, Guangzhou 510006, China*

[2]*Institute of Optical Communication Materials and State Key Laboratory of Luminescent Materials and Devices, South China University of Technology, Guangzhou 510640, China*

**Corresponding author: agwyz@aliyun.com*

Received December 2, 2014; accepted January 16, 2015; posted online May 12, 2015

Cr^{3+}/Yb^{3+} codoped $Y_3Al_5O_{12}$ (i.e., YAG) thin films are prepared by pulsed laser deposition. The films are characterized by X-ray diffraction, atomic force microscopy, transmission electron microscopy, X-ray photoelectron spectroscopy, and photoluminescence spectra. Excitation at 446 or 587 nm, a broadband emission in the range of 610–800 nm, and an intense near-infrared at 1030 nm are obtained, showing cooperative energy transfer from Cr^{3+} to Yb^{3+} ions in the Cr^{3+}/Yb^{3+} codoped YAG thin films; energy transfer efficiency is 71%. The YAG films may have potential application to enhance the efficiency of silicon solar cells.

OCIS codes: 070.4790, 160.2540, 160.5690.
doi: 10.3788/COL201513.060701.

Recently, the rare earth (RE)-ion-doped down-conversion (DC) materials have attracted intensive interest due to their promising application as spectral convertors to improve photovoltaic conversion efficiency. The theoretical limit for the conversion efficiency can be increased from 30% to 39% by applying an ideal down-converting layer on top of Si solar cells[1]. Various trivalent RE ions are possible, such as Pr^{3+}, Ho^{3+}, Er^{3+}, Tb^{3+}, and Tm^{3+} with f–f transition[1–9]. In order to make better use of sunlight, RE ions with f–d transition, such as Ce^{3+}, Eu^{2+}, and Yb^{2+}[10–12]; metal ions, such as Cr^{3+} and Bi^{3+}[13–15]; the host[16] were chosen as the energy donors for Yb^{3+} to realize the broadband spectral conversion. At present, most studies in DC are carried out in powders, crystals, glass ceramics, and glass. For practical application, a down-converting layer should be placed on the front of the p–n junction of solar cells[17]. For powders, the scattering of the incident light becomes a negative factor, which will greatly weaken the absorption of the incident solar light. Regarding crystals, glass ceramics and glass are very fragile and it has big residual stress in the growth processing. On the contrary, it is easy to control film thickness, high transmittance, and also doping concentration of RE ions. Thin-film phosphors can be prepared by many deposition techniques such as pulsed laser deposition (PLD)[18]. In this work, we first explored the efficient broadband energy transfer (ET) from Cr^{3+} to Yb^{3+} ions in $Y_3Al_5O_{12}$ (i.e., YAG) thin films by PLD. The photoluminescence (PL) and photoluminescence excitation (PLE) spectra show that ET happened between Cr^{3+} and Yb^{3+} ions. The decay lifetime of Cr^{3+} and ET efficiency of the films were investigated. These results showed that the efficient DC of Cr^{3+}–Yb^{3+} codoped YAG films might be a good way to improve the efficiency of silicon-based solar cells.

The Cr^{3+}/Yb^{3+} codoped YAG target was prepared by conventional solid-state reaction methods using analytical grade Y_2O_3, Al_2O_3, Yb_2O_3, and Cr_2O_3 powders as the starting materials. These powders were weighted according to the molecular formula $Y_{2.88}Cr_{0.02}Yb_{0.1}Al_5O_{12}$. The starting powders with designed stoichiometric quantities were ball milled for 24 h, then dried and calcinated at 1500°C for 10 h. The resulting powders were pressed into disk pellets and sintered at 1400°C for 6 h. The as-prepared target showed a YAG crystalline phase in the X-ray diffraction (XRD) pattern. The YAG:Cr^{3+}/Yb^{3+} film was grown by PLD on Si(100) substrate at room temperature. PLD process was performed in a vacuum chamber, vacuum degree of 10^{-5} Pa, oxygen pressure of 6.2 Pa, and laser pulse energy power of 300 mJ. After the deposition, the YAG:Cr^{3+}/Yb^{3+} films were annealed at 1000°C for 120 min.

XRD patterns of the samples were recorded with a Rigaku D/max-IIIA X-ray diffractometer ($Cu-K\alpha 1$, $\lambda = 0.15405$ nm). The surface morphology of YAG:Cr^{3+}/Yb^{3+} films was studied by atomic force microscopy (AFM; Digital Instrument Nanoscope IIIa) and transmission electron microscopy (TEM). The chemical state of the films was studied by X-ray photoelectron spectroscopy (XPS) using an ESCALAB250 system. Optical spectroscopy, including emission, excitation spectra, and the decay curves of the specimens, was recorded with an Edingburgh FLS920 fluorescence spectrophotometer at room temperature.

Figure 1 shows the XRD patterns of as-grown and annealed YAG:Cr^{3+}/Yb^{3+} thin films deposited on Si (100) substrates. There is no diffraction peak of as-deposited YAG:Cr^{3+}/Yb^{3+} thin films, indicating that the YAG:Cr^{3+}/Yb^{3+} thin films are amorphous. After annealing at 1000°C, diffraction peaks are clearly observed; main diffraction peaks can be well-assigned to the standard JCPDS card of YAG (JCPDS No. 79-1891) indicating the pure cubic YAG phase with polycrystalline structure. No obvious shifting of peaks or second phase can be detected at the current doping level, indicating that the introduction of Cr^{3+} and Yb^{3+} ions does not change the crystal structure.

Figure 2 shows an AFM image of the YAG:Cr^{3+}/Yb^{3+} thin films annealed at 1000°C. AFM images of the films show a smooth surface with an average grain size of around 16 nm, which is consistent with XRD results. The roughness of the surface of the film is about 8.32 nm.

Figure 3 shows the XPS spectrum of YAG:Cr^{3+}/Yb^{3+} thin film. The XPS survey spectrum confirms the presence of Al, O, Y, Cr, Yb, and C (from carbon pollution).

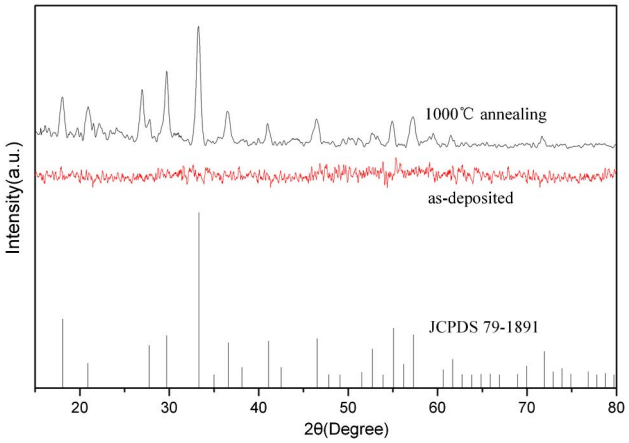

Fig. 1. XRD patterns of YAG:Cr^{3+}/Yb^{3+} thin films.

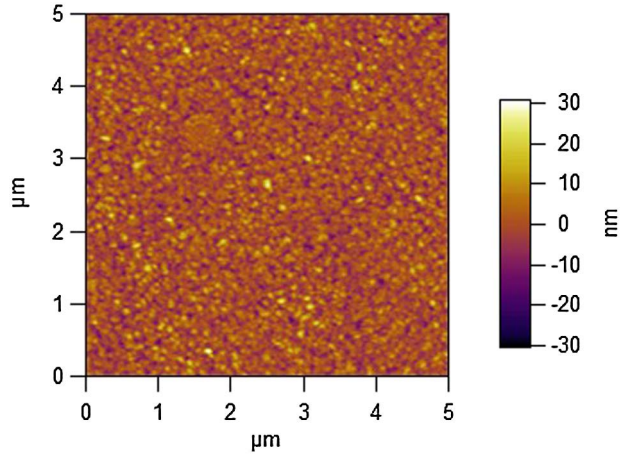

Fig. 2. AFM image of the YAG:Cr^{3+}/Yb^{3+} thin film.

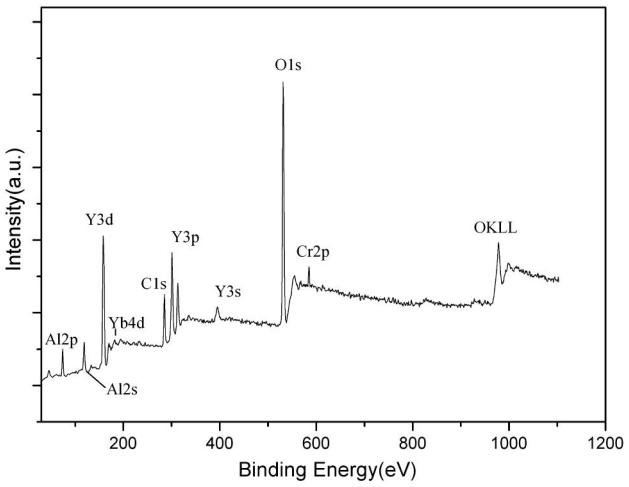

Fig. 3. XPS spectrum of YAG:Cr^{3+}/Yb^{3+} film.

Figure 4(a) shows the cross sectional transmission electron micrograph of the YAG:Cr^{3+}/Yb^{3+} thin films; the thickness of the film was 116 nm. Figure 4(b) shows a high-resolution transmission electron micrograph

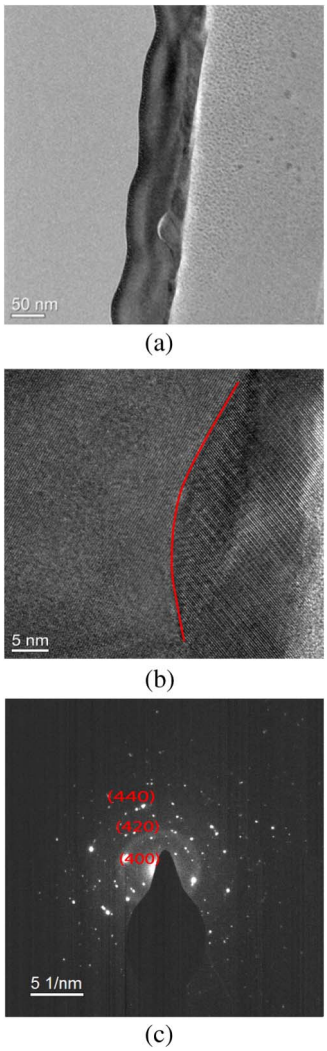

Fig. 4. TEM images of YAG:Cr^{3+}/Yb^{3+} thin films.

(HRTEM), clear lattice can be seen, but there are obvious boundaries, such as the red line which marks the approximate location of the grain boundaries, indicating the presence of a polycrystalline sample. The interplanar spacing of the (400) plane is 0.30 nm. Figure 4(c) presents the corresponding selected area electron diffraction (SAED) pattern; SAED patterns show the (400), (420), and (440) rings typical of the polycrystalline YAG structure.

Figure 5 shows the excitation spectra of YAG:Cr^{3+}/Yb^{3+} films. The excitation spectra show two broad excitation bands at 446 and 595 nm by monitoring $^2E \rightarrow {}^4A_2$ transition of Ce^{3+} at 670 nm and $^2F_{5/2} \rightarrow {}^2F_{7/2}$ transition of Yb^{3+} at 1026 nm; the 446 and 595 nm excitation bands are ascribed to $^4A_2 \rightarrow {}^4T_1$ transition and $^4A_2 \rightarrow {}^4T_2$ transition of Cr^{3+}, respectively. Figure 6 shows the visible emission spectra of YAG:Cr^{3+}/Yb^{3+}. The emission spectrum of YAG:Cr^{3+}/Yb^{3+} films shows a broadband emission in the range of 610–800 nm with a maximum emission at 688 nm assigned to Cr^{3+} $^2E \rightarrow {}^4A_2$ transition under 446 and 587 nm excitation. Figure 7 shows the near-infrared (NIR) emission spectra of YAG:Cr^{3+}/Yb^{3+}. The NIR emission peak centered at 1030 nm originated from $^2F_{5/2} - {}^2F_{7/2}$ transition of Yb^{3+} ions can be clearly observed under the excitations of Cr^{3+}:$^4T_1$ or $^4T_2$ energy levels at 446 or 587 nm, which indicates the ET from Cr^{3+} to Yb^{3+}. For Yb^{3+} single-doped sample, no emission at 900–1100 nm was detected excited by 466 or 587 nm. In addition, the NIR emission spectrum of YAG:Cr^{3+}/Yb^{3+} films excited with simulated sunlight illumination (400–800 nm) is the same as the emission spectrum excited with xenon lamp at 446 or 587 nm of Cr^{3+}; sunlight can be directly applied as a light source for the solar cells' down-converting layer.

ET from Ce^{3+} to Yb^{3+} can be further clarified with the help of decay curves. Figure 8 shows decay curves of 688 nm emission of Cr^{3+} under 466 nm excitation. For the Cr^{3+} single-doped sample, the decay curve of Cr^{3+} exhibits a double-exponential feature. With Yb^{3+} doping,

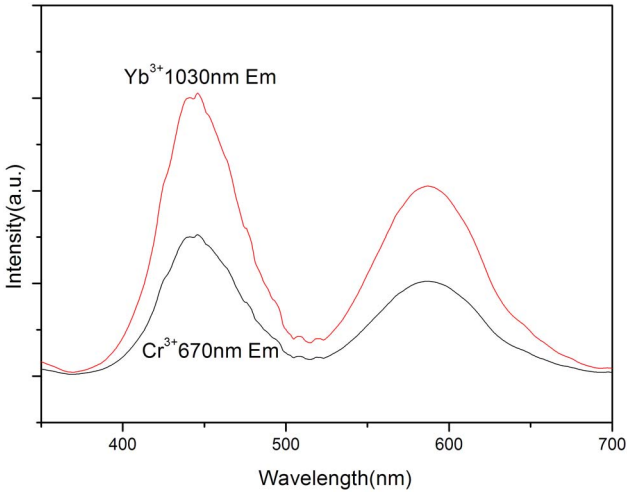

Fig. 5. Excitation spectra of YAG:Cr^{3+}/Yb^{3+} films.

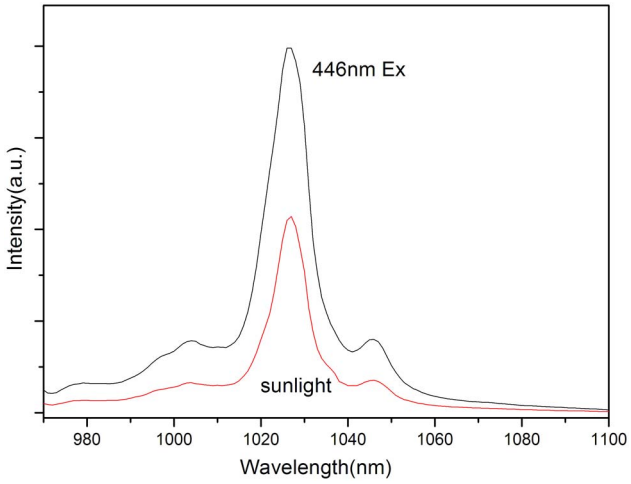

Fig. 7. NIR emission spectra of YAG:Cr^{3+}/Yb^{3+} films.

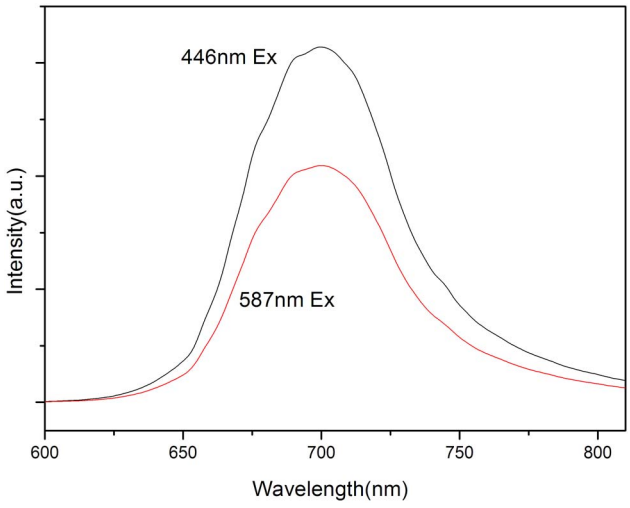

Fig. 6. Visible emission spectra of YAG:Cr^{3+}/Yb^{3+} films.

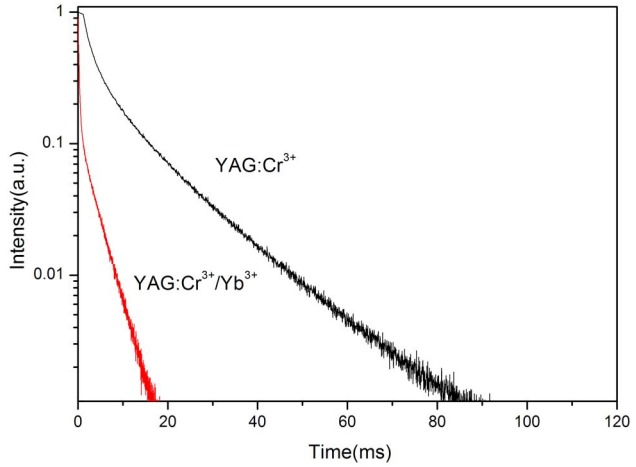

Fig. 8. Decay curves of Cr^{3+} at 688 nm with the excitation at 466 nm for the YAG:Cr^{3+} and YAG:Cr^{3+}/Yb^{3+} films.

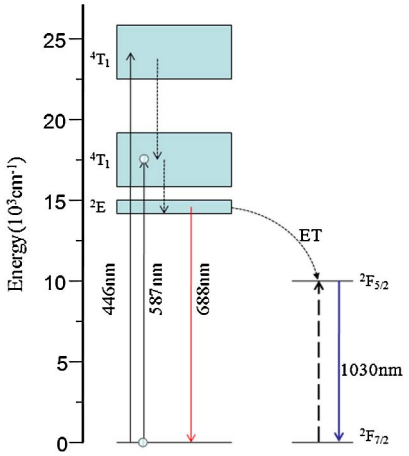

Fig. 9. Energy-level diagram and CET mechanism of Cr^{3+} and Yb^{3+} in YAG:Cr^{3+}/Yb^{3+} films.

the lifetime decreases rapidly and the lifetime of Cr^{3+} decreases, implying the introduction of the extra decay pathway, i.e., cooperative energy transfer (CET) from Cr^{3+} to Yb^{3+}. Figure 9 illustrates the schematic energy levels for Cr^{3+} ion and Yb^{3+} ions in YAG. The Cr^{3+} ion is first excited from $^4A_2$ ground state to $^4T_1$ and $^4T_2$ excitation state, $^4T_1$ followed nonradiative relaxation down to the $^4T_2$ and to further relaxation to ^2E level, or directly from $^4T_2$ to ^2E, then pass to nearly Yb^{3+}:$^2F_{5/2}$ energy level, i.e., Cr^{3+}:$^4T_2 \rightarrow Yb$:$^2F_{5/2}$ and Cr^{3+}:$^4T_1 \rightarrow Yb$:$^2F_{5/2}$. Subsequently, the radiative transition of Yb^{3+}:$^2F_{5/2} \rightarrow {}^2F_{7/2}$ occurs, generating 1030 nm photons.

From the decay curves in Fig. 8, the transfer efficiency η_{ET} can be calculated using[2]

$$\eta_{ET} = 1 - \frac{\int I_{y\mathrm{Yb}^{3+}} \mathrm{d}t}{\int I_{0\mathrm{Yb}^{3+}} \mathrm{d}t}, \quad (1)$$

where I denotes intensity, and y stands for the Yb^{3+} concentration. The obtained ET efficiency for YAG samples is 71%, which is higher than Cr^{3+}–Yb^{3+} codoped YAG crystals (60%)[13], indicating YAG:Cr^{3+}/Yb^{3+} films can as convertors to enhance the solar cell efficiency.

In conclusion, YAG:Cr^{3+}/Yb^{3+} films are investigated as a promising material to enhance the energy conversion efficiency of silicon-based solar cells. Excitation spectra, emission spectra, and decay measurements are performed to prove the CET from Cr^{3+} to Yb^{3+} ions. This evidence implies that YAG:Cr^{3+}/Yb^{3+} films are promising candidates for improving the efficiency of silicon-based solar cells by means of DC.

This work was supported by the National Natural Science Foundation of China (Nos. 11474104 and 51372092) and the China Postdoctoral Science Foundation (No. 2012M511801).

References

1. T. Trupke, M. A. Green, and P. Wurfel, J. Appl. Phys. **92**, 1668 (2002).
2. P. Vergeer, T. J. H. Vlugt, M. H. F. Kox, M. I. Den Hertog, J. P. J. M. van der Eerden, and A. Meijerink, Phys. Rev. B **71**, 014119 (2005).
3. S. Ye, B. Zhu, J. Luo, J. Chen, G. Lakshminarayana, and J. Qiu, Opt. Express **16**, 8989 (2008).
4. K. Deng, T. Gong, L. Hu, X. Wei, Y. Chen, and M. Yin, Opt. Express **19**, 1749 (2011).
5. J. Di, X. Xu, C. Xia, D. Li, D. Zhou, Q. Sai, L. Wang, and J. Xu, Phys. B Condensed Matter **408**, 1 (2013).
6. K. Deng, X. Wei, X. Wang, Y. Chen, and M. Yin, Appl. Phys. B **102**, 555 (2011).
7. Q. Zhang, G. Yang, and Z. Jiang, Appl. Phys. Lett. **91**, 051903 (2007).
8. X. Yi, H. Lin, C. Chen, and S. Zhou, Chin. Opt. Lett. **12**, S11603 (2014).
9. X. Liu, S. Xiao, Z. Xiang, B. Zhou, Q. Wen, X. Yang, and X. Jin, Chin. Opt. Lett. **11**, 122602 (2013).
10. D. Chen, Y. Wang, Y. Yu, P. Huang, and F. Weng, J. Appl. Phys. **104**, 116105 (2008).
11. J. Zhou, Y. Teng, G. Lin, X. Xu, Z. Ma, and J. Qiu, J. Electrochem. Soc. **157**, B1146-8 (2010).
12. Y. Teng, J. Zhou, X. Liu, S. Ye, and J. Qiu, Opt. Express **18**, 9671 (2010).
13. S. Ye, J. Zhou, S. Wang, R. Hu, D. Wang, and J. Qiu, Opt. Express **21**, 4167 (2013).
14. P. Liu, J. Liu, X. Zheng, H. Luo, X. Li, Z. Yao, X. Yu, X. Shi, B. Hou, and Y. Xia, J. Mater. Chem. C **2**, 5769 (2014).
15. Y. Zhydachevskii, L. Lipińska, M. Baran, M. Berkowski, A. Suchocki, and A. Reszka, Mater. Chem. Phys. **143**, 622 (2014).
16. X. Cheng, L. Su, Y. Wang, X. Zhu, and X. Wei, Opt. Mater. **34**, 1102 (2012).
17. A. D. Vos, A. Szymanska, and V. Badescu, Energy Convers. Manage. **50**, 328 (2009).
18. J. Hu, Q. Li, X. Lin, Y. Liu, J. Long, L. Wang, and H. Tang, Chin. Opt. Lett. **12**, 072201 (2014).